J Membrane Biol (2010) 237:1–11
DOI 10.1007/s00232-010-9298-6

ORIGINAL ARTICLES

Formation of Very Large Conductance Channels by *Bacillus cereus* Nhe in Vero and GH_4 Cells Identifies NheA + B as the Inherent Pore-Forming Structure

Trude M. Haug · Sverre L. Sand · Olav Sand · Danh Phung · Per E. Granum · Simon P. Hardy

Received: 7 June 2010 / Accepted: 13 August 2010 / Published online: 7 September 2010

Abstract The nonhemolytic enterotoxin (Nhe) produced by *Bacillus cereus* is a pore-forming toxin consisting of three components, NheA, -B and -C. We have studied effects of Nhe on primate epithelial cells (Vero) and rodent pituitary cells (GH_4) by measuring release of lactate dehydrogenase (LDH), K^+ efflux and the cytosolic Ca^{2+} concentration ($[Ca^{2+}]_i$). Plasma membrane channel events were monitored by patch-clamp recordings. Using strains of *B. cereus* lacking either NheA or -C, we examined the functional role of the various components. In both cell types, NheA + B + C induced release of LDH and K^+ as well as Ca^{2+} influx. A specific monoclonal antibody against NheB abolished LDH release and elevation of $[Ca^{2+}]_i$. Exposure to NheA + B caused a similar K^+ efflux and elevation of $[Ca^{2+}]_i$ as NheA + B + C in GH_4 cells, whereas in Vero cells the rate of K^+ efflux was reduced by 50% and $[Ca^{2+}]_i$ was unaffected. NheB + C had no effect on either cell type. Exposure to NheA + B + C induced large-conductance steps in both cell types, and similar channel insertions were observed in GH_4 cells exposed to NheA + B. In Vero cells, NheA + B induced channels of much smaller conductance. NheB + C failed to insert membrane channels. The conductance of the large channels in GH_4 cells was about 10 nS. This is the largest channel conductance reported in cell membranes under quasi-physiological conditions. In conclusion, NheA and NheB are necessary and sufficient for formation of large-conductance channels in GH_4 cells, whereas in Vero cells such large-conductance channels are in addition dependent on NheC.

Keywords *Bacillus cereus* · Pore-forming toxin · Nonhemolytic enterotoxin · Large-conductance channel · Vero cell · GH_4 cell

T. M. Haug (✉) · S. L. Sand · O. Sand
Department of Molecular Biosciences, University of Oslo, Post Box 1041, 0316 Oslo, Norway
e-mail: t.m.haug@imbv.uio.no

D. Phung · P. E. Granum · S. P. Hardy
Department of Food Safety and Infection Biology, Norwegian School of Veterinary Science, Post Box 8146 Dep, 0033 Oslo, Norway

Introduction

Many bacteria secrete pore-forming protein toxins (PFTs) that can disrupt the ionic gradients and abolish the potential difference across the plasma membrane of eukaryotic cells. Usually, the unregulated flux of ions and molecules through the pores results in osmotic lysis of the cell, although cells may repair small lesions (Parker and Feil 2005). PFTs are classified as either α-PFTs or β-PFTs depending on the α-helical or β-sheet structures that form the transmembrane pore. PFTs are secreted in water-soluble form and oligomerize upon binding to target cells, in a manner that assembles sufficient amphipathic stretches to span the membrane (Gonzalez et al. 2008; Anderluh and Lakey 2008). Most bacterial PFTs are homo-oligomeric, exemplified by *Staphylococcus aureus* α-toxin, a β-PFT for which a crystal structure has been obtained (Montoya and Gouaux 2003). However, hetero-oligomeric PFTs also exist, as exemplified by the β-PFT leukocidins of *S. aureus* (Miles et al. 2002), which form binary complexes.

Bacillus cereus produces several cytolytic PFTs, including cytolysin K (CytK), hemolysin BL (Hbl) and nonhemolytic enterotoxin (Nhe), all of which have been implicated as the causes of the diarrheal type of food poisoning (Arnesen et al. 2008). While CytK is a single

protein, Hbl and Nhe are three-component toxins. Nhe was identified in *B. cereus* following a large food-poisoning outbreak in Norway in 1995. This strain (NVH75/95) was cytotoxic despite lacking CytK and Hbl (Lund and Granum 1996), thus permitting the identification of Nhe. The three separate Nhe proteins, NheA, -B and -C, are all 36–41 kDa in size and have sequence homology (20–44%) (see Fagerlund et al. 2008 for exact sequence identities) between the three components as well as the related Hbl proteins. To date, all studies have shown that all three Nhe components are needed to induce cytotoxicity in primate epithelial cells (Lindback et al. 2004), i.e., clonal kidney cells from African green monkey (Vero cells) and clonal colorectal cells from human (Caco-2 cells) (Fagerlund et al. 2008). However, the function of the individual Nhe components remains largely unknown. No intracellular target has been identified for Nhe since it exerts rapid membrane permeabilization and lysis of both nucleated cells and erythrocytes, consistent with Nhe-forming pores in the plasma membrane, thereby inducing osmotic cell lysis (Fagerlund et al. 2008).

Recently, homology modeling of NheB and NheC with one of the components of the related hemolysin of *B. cereus*, HblB, uncovered a striking similarity with the single-protein toxin cytolysin A (ClyA) (Fagerlund et al. 2008; Madegowda et al. 2008), despite weak sequence similarity. ClyA is an α-PFT produced by invasive enteric pathogens such as *Escherichia coli Salmonella typhi* and *Shigella flexneri* (Ludwig et al. 1995; Oscarsson et al. 2002). The crystal structures of the aqueous and membrane-bound forms of ClyA have been published, revealing a dodecameric pore structure in detergent micelles (Mueller et al. 2009). In addition to structural similarity, Nhe shows phenotypic properties that mirror those of ClyA; i.e., both are cytolytic to epithelia and form large-conductance channels in planar lipid bilayers (Ludwig et al. 1995, 1999; Oscarsson et al. 2002; Lai et al. 2000; Fagerlund et al. 2008). Cytolysis by both toxins can be reduced by addition of large-molecular weight osmotic protectants, indicating that the epithelial cells lyse following channel formation.

To date, release of lactate dehydrogenase (LDH) from Vero and Caco-2 cells has been used to monitor the cytotoxicity of Nhe (Fagerlund et al. 2008). LDH release represents cell lysis, i.e., an end-stage event. As channel insertions have not been directly demonstrated for Nhe in native cell membranes, we examined membrane effects of Nhe on Vero cells and clonal rat pituitary cells (GH_4 cells) using a variety of additional techniques. Membrane permeabilization was monitored by measuring K^+ efflux and the cytosolic Ca^{2+} concentration ($[Ca^{2+}]_i$), whereas patch-clamp recordings were used to reveal insertion of single channels in the plasma membrane. Furthermore, we examined the functional roles of the three Nhe components by using different strains of *B. cereus* that lack one of the proteins.

We show that the Nhe toxin complex forms large-conductance channels in the plasma membrane of the target cells. To our knowledge, the recorded channel conductance is the highest that has so far been reported in cell membranes under quasi-physiological conditions. In GH_4 cells, only two of the three Nhe components (NheA and -B) are required for channel formation in the plasma membrane, whereas in Vero cells and the target cells for food poisoning (intestinal epithelial cells) the third component (NheC) has a cell type-specific, permissive action on channel insertion.

Materials and Methods

Culture of Clonal Vero Cells

The epithelial Vero cell line was derived from a normal kidney of African green monkey (*Cercopithecus aethiops*) (Liebhaber et al. 1967). Vero cells were grown as monolayer cultures in plastic tissue culture flasks containing Dulbecco's modified Eagle medium (DMEM) supplemented with newborn calf serum (5%), penicillin (50 μg ml^{-1}), streptomycin (50 μg ml^{-1}) and L-glutamine (2 mM) at 37°C in a humidified atmosphere of 5% CO_2 and 95% air. Cells for electrophysiological studies were seeded in 35-mm Petri dishes 1–5 days before recording. Cells for microfluorometric studies were seeded in 35-mm Petri dishes with a glass bottom.

Culture of Clonal Rat Anterior Pituitary GH_4 Cells

The GH strains of rat pituitary tumor cells were established by Tashjian et al. (1968). These cells spontaneously synthesize and secrete prolactin and/or growth hormone and are electrically excitable. In the present study, we used the GH_4C_1 subclone. Cells were grown as monolayer cultures in plastic tissue culture flasks containing Ham's F-10 medium supplemented with horse serum (7.5%), fetal calf serum (2.5%), penicillin (50 U ml^{-1}) and streptomycin (100 μg ml^{-1}) at 37°C in a humidified atmosphere of 5% CO_2 and 95% air. Cells for electrophysiological studies were seeded in 35-mm dishes 2–7 days prior to recording. Cells for microfluorometric studies were seeded in 35-mm Petri dishes with a glass bottom.

Bacillus cereus Strains and Crude Toxin Preparation

Three naturally occurring strains of *B. cereus*, producing different combinations of the three Nhe components, were used. All of these strains lack Hbl and CytK (Lindback et al.

2010). *B. cereus* NVH75/95 is the strain that was isolated following a large food-poisoning outbreak in Norway (Lund and Granum 1996). This strain produces all three Nhe components, i.e., NheA, -B and -C. *B. cereus* MHI1672 lacks NheC but produces NheA and -B, whereas *B. cereus* MHI1761 produces NheB and -C but lacks NheA. Details of the toxin titers are given elsewhere (Lindback et al. 2010).

The *B. cereus* strains were grown in a modified version of the casitone glycerol yeast autolysate medium (CGY) described by Beecher and Wong (1994), i.e., 2% casein hydrolysate (Merck, Whitehouse Station, NJ), 0.6% yeast extract (Sigma, St. Louis, MO), 30 mM sucrose, 15 mM $(NH_4)_2SO_4$, 80 mM K_2HPO_4, 44 mM KH_2PO_4, 4 mM $Na_3C_6H_5O_7$ (trisodium citrate) and 17 mM $MgSO_4$. A 2% inoculum of an overnight culture was incubated at 32°C in 50 ml CGY (in a 250-ml flask) and shaken at 100 rpm for 5–6 h until transition into the stationary growth phase at a cell density of about 10^8 ml^{-1}. The supernatant was centrifuged and filtered through a 0.2-μm membrane filter and stored in aliquots at −80°C. Prior to experiments, the supernatant was diluted 40 or 80 times in experimental extracellular solution (EC; see below, Electrophysiology) and kept on ice until used. The monoclonal antibody (Mab) 1E11 against NheB is able to neutralize the cytotoxic activity of the diluted Nhe-containing supernatant at a concentration of 10 μg ml^{-1} (Dietrich et al. 2005). In the present study, Mab 1E11 was used to confirm the specificity of the response to the crude toxin preparation and to evaluate the functional role of NheB in the Nhe-induced membrane permeabilization.

LDH Release

Cellular release of large cytosolic molecules is a sign of cell membrane disruption, and LDH leakage from Vero and GH_4 cells was measured in order to reveal cell lysis. Cells were grown in 24-well microplates for 48 h and tested at 90–100% confluence. Cell culture medium was replaced with pre-warmed 2 ml bathing solution containing 135 mM NaCl, 15 mM HEPES, 1 mM $MgCl_2$, 1 mM $CaCl_2$ and 10 mM glucose, adjusted to pH 7.2 with Trisma base. Cells were equilibrated for at least 15 min at 37°C before replacement with 1 ml bathing solution containing 25 μl *B. cereus* culture supernatant. LDH in the bathing solution was measured at timed intervals using an ADVIA 1650 autoanalyzer (Bayer, Leverkusen, Germany). Total-cell LDH was measured by replacing the entire cell bathing solution of control cells with 1 ml buffer containing 1% (v/v) Triton X-100.

K^+ Efflux from Vero and GH_4 Cells

Cell suspensions were prepared from monolayer cultures using conventional tissue culture protocols (trypsin + EDTA) and resuspended gently in an extracellular buffer solution in which sodium was replaced with choline to aid selectivity of the K^+-selective electrode. Cells were allowed to equilibrate in the new buffer for 15 min at 37°C prior to assay. The buffer contained 150 mM choline-Cl, 15 mM HEPES, 1 mM $CaCl_2$, 1 mM $MgCl_2$ and 10 mM glucose, pH 7.2 adjusted with Trisma base. All recordings were carried out at 27°C. K^+ efflux was monitored using a combination electrode (DC239-K; Mettler-Toledo, Greifensee, Switzerland) in a 2.5-ml suspension of 10^6 cells, gently stirred using a magnetic bead. The electrode voltage, which reflects the K^+ concentration in the solution, was fed to a Seven Multi Ion Meter (Mettler-Toledo) connected to a DI 158U (DataQ Instruments, Akron, OH) interface. Recordings were sampled at 2 Hz and stored in a computer using Windaq software (DataQ Instruments). Toxin preparations were dialyzed overnight at 4–6°C in distilled water containing 15 mM HEPES and 1 mM EDTA adjusted to pH 7.2 with Trisma base in order to reduce the K^+ concentration. Fifty microliters of the various toxin preparations were added to the cell suspensions, and the K^+ concentration was recorded for 10 min, after which 25 μl of 2.5% Triton X-100 in water was added as a lytic control. Triton X-100 at this concentration did not induce any change in voltage in the absence of cells when added to the choline buffer solution.

Microfluorometry of Fura-2-Loaded Cells

Cells were loaded with the fluorescent Ca^{2+} indicator fura-2 by exposure to 5 μM fura-2/AM (Molecular Probes, Eugene, OR) in EC (see below, Electrophysiology) for 40 min at 37°C, followed by washout of the fura-2 ester and further 30-min incubation at room temperature. Then, cells were mounted on an Olympus inverted microscope, forming the central part of the Olympus OSP-3 system for dual excitation fluorometry (Olympus, Tokyo, Japan). The excitation light was switched at 200 Hz between 360 and 380 nm using a rotating mirror. The emitted fluorescence was recorded at 510 nm with a photomultiplier, and the measurements were restricted to single cells by a pinhole diaphragm. The ratio between emissions at the two different excitation wavelengths (F360/F380) reflects $[Ca^{2+}]_i$. The emission at the isosbestic wavelength 360 nm is independent of $[Ca^{2+}]_i$ and, thus, monitors the cytosolic concentration of the fluorophore ($[fura\text{-}2]_i$). Cells were exposed to Nhe by pressure ejection (about 1 kPa) from a micropipette (inner tip diameter 1–2 μm) placed about 40 μm from the cell or by leakage from the pipette at a distance of about 15 μm. No artefacts were observed when ejecting or leaking normal EC onto cells from these distances.

Electrophysiology

Electrophysiological recordings were performed in the following EC: 150 mM NaCl, 5 mM KCl, 2.4 mM $CaCl_2$, 1.3 mM $MgCl_2$, 10 mM glucose and 10 mM HEPES, adjusted to pH 7.4 by NaOH. Patch electrodes were filled with the following solution: 120 mM CH_3O_3SK, 20 mM KCl, 20 mM sucrose and 10 mM HEPES, adjusted to pH 7.2 by NaOH. Standard whole-cell and excised outside-out patch-clamp recordings were used to measure membrane potential and membrane currents (Hamill et al. 1981). In both configurations, the toxin is applied to the outside of the membrane. Since we found channel insertion to be a rare event, we mostly employed whole-cell recordings, increasing the chance of channel insertion by increasing the total membrane surface. Patch-clamp recordings were carried out at room temperature. Patch electrodes were made from borosilicate glass with filament and heat-polished before use, and the electrode resistance was 4–6 MΩ. Electrodes were connected to an EPC-7 patch-clamp amplifier (HEKA, Lambrecht/Pfaltz, Germany) controlled by the software PClamp 9.2 (Axon Instruments, Union City, CA). Recorded signals were digitized at 4–10 kHz, filtered at one-third of the sampling rate and stored on a computer. Recordings were not adjusted for the electrode junction potentials. Membrane currents flowing from the extracellular to the cytoplasmic side were defined as negative and displayed as downward deflections in the current traces. Data were analyzed using PClamp 9.2 and Origin 7.0 (OriginLab, Northampton, MA). Cells and excised patches were exposed to Nhe by pressure ejection or leakage from a micropipette, as described above.

Results

Nhe Induces LDH Release in Both Vero and GH_4 Cells

Previous studies have shown that in combination the three components of Nhe induce time-dependent release of LDH from Vero cells, reflecting osmotic cell lysis (Fagerlund et al. 2008). To test whether Nhe also lyses GH_4 cells, we repeated the LDH release experiments on both Vero and GH_4 cells. When exposed to a crude filtrate of supernatant from *B. cereus* NVH75/95 (NheA + B + C), both Vero and GH_4 cells released LDH to the same extent as when exposed to Triton X-100 (Fig. 1). To rule out possible lytic activity from other, unidentified components in the filtrate, we tested the effect of the specific monoclonal antibody against NheB, Mab 1E11. If the residual leak of LDH is taken into account, Mab 1E11 effectively abolished the cytolytic response (Fig. 1). Thus, the cytotoxic effect of the culture supernatant of NVH75/95 is dependent on NheB.

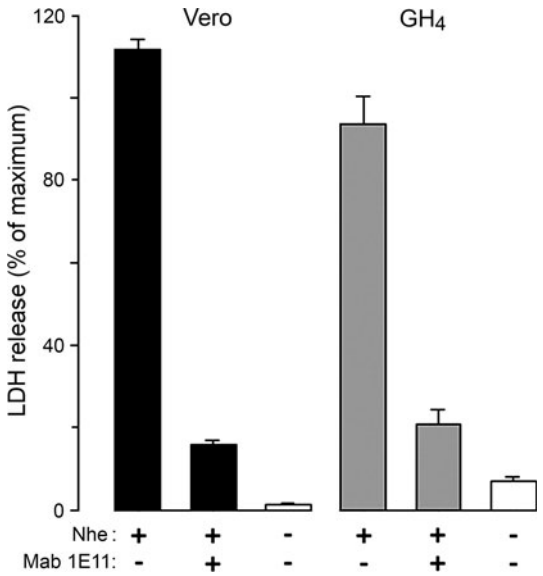

Fig. 1 LDH release from Vero (columns *1–3*) and GH_4 (columns *4–6*) cells exposed to culture supernatant of *B. cereus* NVH75/95 (NheA + B + C). LDH in the bathing solution was measured after 30-min incubation with and without addition of 10 μg ml^{-1} of the specific Mab 1E11 against NheB (mixed with the toxin immediately prior to addition to the cells), as indicated below the columns. Results (mean ± SE, $n = 3$ for each condition) are expressed as percentage of the maximum LDH released by 1% (v/v) Triton X-100. Cells exposed to buffer alone are represented by *open columns*

Nhe Induces K^+ Efflux in Vero and GH_4 Cells

The membrane permeability of K^+ in cells exposed to Nhe was examined using a K^+-selective electrode. Figure 2 shows the time course of K^+ efflux from Vero cell suspensions following exposure to culture supernatants of *B. cereus* strains NVH75/95 and MHI1672. Exposure to all three Nhe components (NVH75/95) induced the greatest rate of K^+ efflux in Vero cells. NheA + B (MHI1672) significantly increased the K^+ efflux rate but to a lesser degree than NheA + B + C. No significant change in efflux rate was detected during exposure to NheB + C (MHI1761) relative to the efflux in control buffer. In GH_4 cells, exposure to either all three Nhe components (NVH75/95) or just NheA + B (MHI1672) yielded similar K^+ efflux rates; but as with Vero cells, exposure to NheB + C (MHI1761) gave no significant increase in K^+ efflux. The data from all of the K^+ efflux recordings are summarized in Table 1. These data indicate that NheA, like NheB, is an absolute requirement for the Nhe-induced membrane permeabilization, while the contribution of NheC in this process seems to be dependent on cell type.

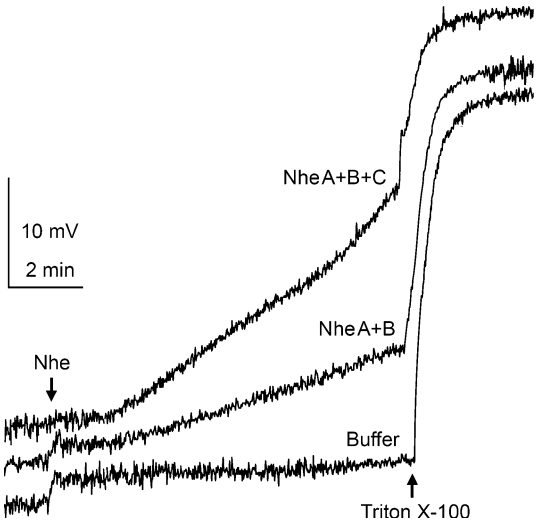

Fig. 2 K^+ efflux from Vero cells exposed to culture supernatants of *B. cereus* NVH75/95 (NheA + B + C) and MHI1672 (NheA + B) and dialysis buffer (control). Ten minutes after adding 50 µl of the culture supernatants (indicated by *arrow*) to the 2.5 ml bathing solution (150 mM choline chloride buffer, pH 7.2, 27°C) containing a suspension of 10^6 Vero cells, Triton X-100 was added to a final concentration of 0.025% (v/v). K^+ release was monitored as change in voltage recorded by a K^+-selective electrode in the bath. Traces are representative of at least three separate experiments for each condition. Traces have been adjusted vertically (original traces overlaid each other at the start) to aid clarity

Table 1 K^+ efflux from Vero and GH_4 cells induced by *B. cereus* strains expressing different combinations of Nhe components

B. cereus (toxin combination)	K^+ efflux (ΔmV)	
	Vero cells	GH_4 cells
NVH75/95 (NheA + B + C)	18.0 ± 2.5* (3)	17.0 ± 3.1* (3)
MHI1672 (NheA + B)	8.6 ± 1.2* (3)	15.0 ± 3.0* (4)
MHI1761 (NheB + C)	2.6 ± 1.2 (3)	5.3 ± 2.1 (4)
Dialysis buffer	2.0 ± 0.4 (4)	2.7 ± 1.4 (3)

Results are expressed as change in voltage (mean ± SE) recorded by a K^+-selective electrode in the bath after 10-min exposure to the *B. cereus* culture supernatants. The recording chamber contained 10^6 cells suspended in 2.5 ml choline-based bathing solution, and 50 µl of the various supernatants was added as indicated. The number of experiments is given in *parentheses*

* Values significantly different ($P < 0.05$) from the dialysis buffer control (one-way ANOVA and Holm-Sidak pairwise comparisons)

Nhe Increases $[Ca^{2+}]_i$ Followed by Leakage of Fura-2

To improve the time resolution of the detection of membrane permeabilization over that obtained by monitoring LDH release and K^+ efflux, where the results represent average values from a large cell population, we employed microfluorometry to continuously monitor both $[Ca^{2+}]_i$ and fluorophore concentration in single cells loaded with fura-2. Among the inorganic ions in physiological solutions, Ca^{2+} has the greatest electrochemical gradient across the cell membrane, and measurement of $[Ca^{2+}]_i$ elevation is a sensitive method for detecting membrane permeabilization. After 1–2 min of exposure to NheA + B + C (NVH75/95), both Vero and GH_4 cells displayed a rapid increase of $[Ca^{2+}]_i$ (Fig. 3a, c). After a subsequent delay of 50–60 s, F360 started to decline at a significantly higher rate than that due to photobleaching, indicating diffusional loss of the relatively large fura-2 molecules from the cytosol due to a leaky cell membrane. Similar results were obtained from all ten cells of each cell type that were exposed to NheA + B + C. The specificity of the observed effect was verified by the total lack of response in cells ($n = 5$ for each cell type) exposed to NheA + B + C incubated with the specific Mab 1E11 against NheB (Fig. 3b, d), which also confirms that the Nhe-induced membrane permeabilization is dependent on NheB. It was a common observation that the GH_4 cells displayed marked oscillations of $[Ca^{2+}]_i$ during the first phase of the response to Nhe. This might be due to the presence of voltage-gated Ca^{2+} channels and Ca^{2+}-activated K^+ channels in this cell line. A moderate initial permeabilization probably depolarized the cell, and the oscillations may represent the ensuing Ca^{2+} influx through Ca^{2+} channels that were subsequently closed by repolarization caused by outward K^+ current. However, such effects were soon overridden by the massive permeabilization caused by Nhe.

It has recently been reported that the pore-forming exotoxin streptolysin-O produced by hemolytic streptococci may elevate $[Ca^{2+}]_i$ by inducing release of Ca^{2+} from intracellular stores, subsequent to activation of phospholipase C (Usmani et al. 2010). To examine if this might also be the case for the Nhe-induced elevation of $[Ca^{2+}]_i$, five GH_4 cells were exposed to NheA + B + C in Ca^{2+}-free extracellular solution. Under such conditions, no significant increase in $[Ca^{2+}]_i$ was detected (Fig. 4). However, Nhe-induced leakage of fura-2 was still observed after some delay, confirming that NheA + B + C had permeabilized the membrane also in the absence of extracellular Ca^{2+}, which is consistent with our earlier finding that permeation to propidium iodide by NheA + B + C was not dependent on extracellular Ca^{2+} (Fagerlund et al., 2008). These results support our assumption that the Nhe-induced elevation of $[Ca^{2+}]_i$ is due to influx of extracellular Ca^{2+} through a permeabilized cell membrane. The requirement for the individual Nhe components in order to elevate $[Ca^{2+}]_i$ was examined by comparing the effects of the three strains of *B. cereus* (Fig. 5). Exposure to NheA + B (MHI1672) increased $[Ca^{2+}]_i$ to saturating levels in GH_4 cells ($n = 3$) but had no effect on $[Ca^{2+}]_i$ in Vero cells ($n = 4$). The contribution of NheA was examined by applying NheB + C (MHI1761), which caused no increases in $[Ca^{2+}]_i$ in either Vero cells or GH_4 cells

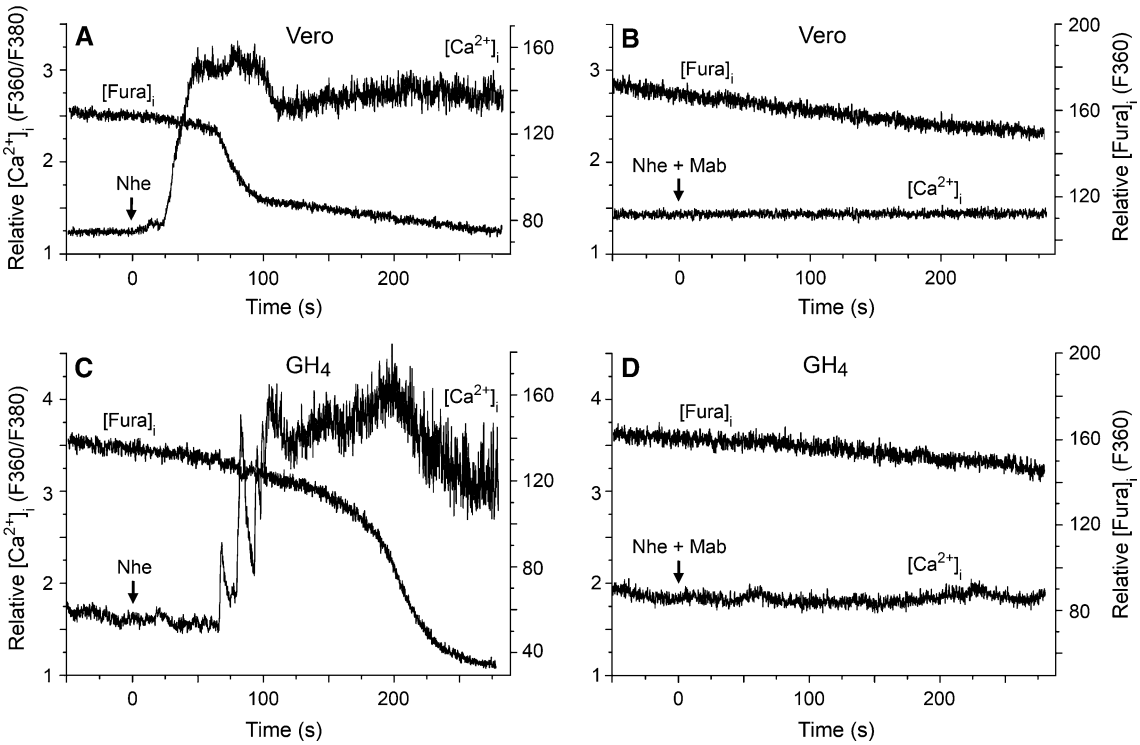

Fig. 3 Microfluorometric recordings of $[Ca^{2+}]_i$ and $[fura\text{-}2]_i$ from fura-2-loaded Vero and GH_4 cells exposed to NheA + B + C (NVH75/95). The ratio between emissions at the excitation wavelengths 360 and 380 nm reflects $[Ca^{2+}]_i$, whereas emission at the isosbestic wavelength 360 nm reflects $[fura\text{-}2]_i$. Nhe was applied continuously by pressure ejection onto the cells from the time indicated by the *arrows*, either in the absence (**a**, **c**) or in the presence (**b**, **d**) of the specific Mab 1E11 against NheB. Nhe induced rapid elevation of $[Ca^{2+}]_i$ after a delay of 50–90 s, followed by cellular loss of fluorochrome, indicating massive membrane permeabilization. These effects were completely blocked by the Mab

($n = 6$ for both cell types). Together with the results from the experiments using the monoclonal antibody against NheB, these data show that all three Nhe components are necessary for permeabilization of the cell membrane to Ca^{2+} in Vero cells, whereas only NheA and NheB are required in GH_4 cells. Note, however, that permeabilization to K^+ by NheA + B was common to both cells types, as shown in the K^+ efflux data (Table 1, Fig. 2).

Nhe Induces Gigantic Steps in Membrane Conductance

To directly monitor the membrane permeabilization induced by Nhe, we employed whole-cell and outside-out patch-clamp recordings from Vero and GH_4 cells. Using quasi-physiological conditions, exposure of cells to NheA + B + C (NVH75/95) resulted in large steps in the holding current in voltage-clamped cells or outside-out membrane patches held at −40 mV (close to the natural resting membrane potential). Figure 6 shows representative current recordings from Vero cells (Fig. 6a) and GH_4 cells (Fig. 6d) exposed to NheA + B + C. In both cell types, a series of large, negative current steps, corresponding to channel insertions, appeared 1–3 min after the start of

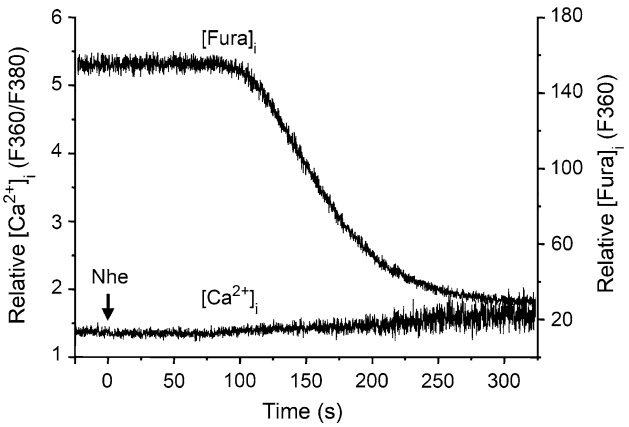

Fig. 4 Microfluorometric recordings of $[Ca^{2+}]_i$ and $[fura\text{-}2]_i$ from a fura-2-loaded GH_4 cell exposed to NheA + B + C (NVH75/95) in Ca^{2+}-free extracellular solution. The ratio between emissions at the excitation wavelengths 360 and 380 nm reflects $[Ca^{2+}]_i$, whereas emission at the isosbestic wavelength 360 nm reflects $[fura\text{-}2]_i$. NheA + B + C was applied continuously by pressure ejection onto the cell from the time indicated by the *arrow*. NheA + B + C induced massive membrane permeabilization, resulting in cellular loss of fluorochrome, but no increase in $[Ca^{2+}]_i$. Therefore, the elevation of $[Ca^{2+}]_i$ observed in normal extracellular solution is caused by influx of Ca^{2+} and not Ca^{2+} release from intracellular stores

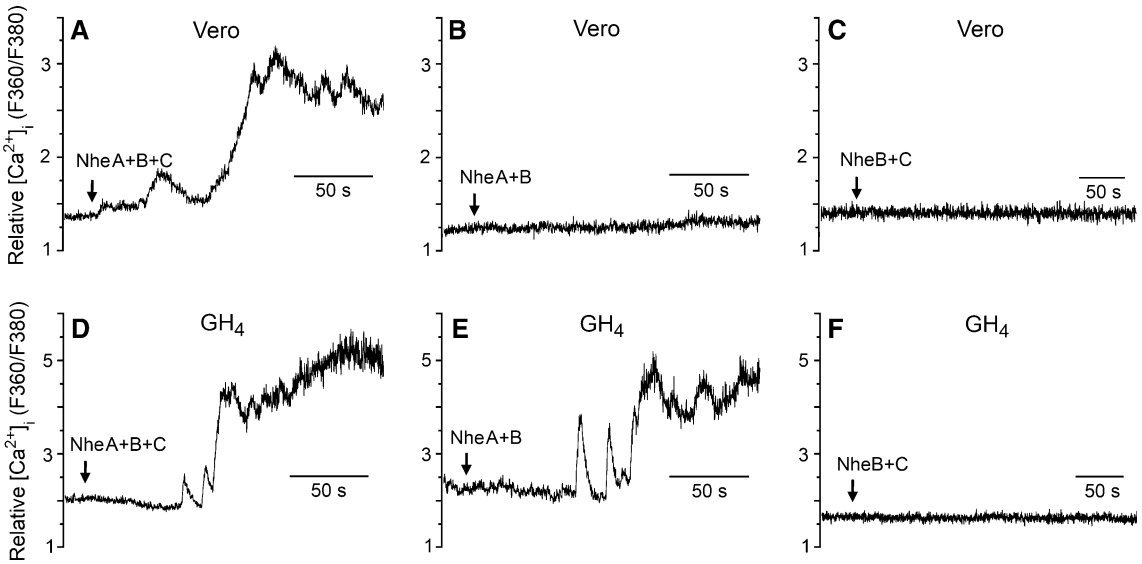

Fig. 5 Microfluorometric recordings of $[Ca^{2+}]_i$ from fura-2-loaded Vero and GH_4 cells exposed to NheA + B + C (NVH75/95), NheA + B (MHI1672) and NheB + C (MHI1761). The ratio between emissions at the excitation wavelengths 360 and 380 nm reflects $[Ca^{2+}]_i$. Nhe was applied continuously by pressure ejection onto the cells from the time indicated by the *arrows*. NheA + B + C induced rapid elevation of $[Ca^{2+}]_i$ in both Vero and GH_4 cells (**a**, **d**). NheA + B induced elevation of $[Ca^{2+}]_i$ only in GH_4 cells (**b**, **e**), while NheB + C had no effect on $[Ca^{2+}]_i$ in either of the tested cell types (**c**, **f**)

exposure to the toxin. Given that channel insertions were relatively rare events, variation in time before detection of insertions is expected. However, there did not appear to be any obvious correlation between time to the first channel insertion and the different toxin combinations or cell types, but this was not analyzed further. At a holding potential of −40 mV, the average size of the initial current step for each cell was −414 ± 93 pA (SD, $n = 5$) for Vero cells and −425 ± 104 pA (SD, $n = 7$) for GH_4 cells. However, the average size of the first three steps from each cell was −273 ± 132 pA ($n = 15$) for Vero cells and −373 ± 103 pA ($n = 21$) for GH_4 cells. Hence, the amplitudes of the subsequent channel insertions tended to get smaller with time. The cause of this time-dependent reduction in channel size is unclear.

To determine the Nhe components that are necessary for pore formation, we also tested the effects of NheA + B (MHI1672) and NheB + C (MHI1761). Whole-cell recordings from Vero cells exposed to NheA + B ($n = 5$) displayed steps of considerably smaller amplitude than those induced by NheA + B + C (NVH75/95) (Fig. 6b). In contrast, GH_4 cells exposed to NheA + B ($n = 9$) yielded large-conductance channels comparable to those inserted by NheA + B + C (Fig. 6e). The requirement for NheA was examined by exposing the cells to NheB + C, which failed to induce any significant conductance steps in either Vero ($n = 5$) (Fig. 6c) or GH_4 ($n = 5$) (Fig. 6f) cells. Thus, NheA + B and NheA + B + C form very large channels of similar conductance in GH_4 cells, demonstrating that insertion of such channels in the GH_4 cell membrane is independent of NheC. However, also NheC is required for insertion of full-sized channels in the Vero cell membrane, indicating an accommodating action of this Nhe component.

The experiments described above revealed that the properties of NheA + B + C channels inserted in Vero and GH_4 cells were rather similar. Therefore, a complete *I–V* curve for the channel was established only for GH_4 cells, which form gigaseals with the patch electrodes much more readily than Vero cells. Whole-cell voltage-clamp recordings were obtained from cells kept at different holding potentials. For each cell, the initial current step was used for construction of the single channel *I–V* curve (Fig. 7). Five GH_4 cells were exposed to the toxin at each holding potential. The *I–V* curve is linear and lacks rectification, at least within the tested voltage range. The slope of the regression line represents a single-channel conductance of 10 nS with a reversal potential of 0 mV, indicating an unselective channel, as expected for a channel this size. Using current clamp recordings, it was observed that a single-channel insertion event was sufficient to nullify the membrane potential (data not shown), consistent with the activity of a very large conductance channel.

Similar experiments were also performed using NheA + B. As expected from the size of the induced current steps (Fig. 6e), the conductance of the channels formed by NheA + B in GH_4 cells was also 10 nS, identical to that of the channels inserted by NheA + B + C (Fig. 7). This is an extremely high unitary conductance and more than ten times the previously reported Nhe-induced channels in planar lipid bilayers (Fagerlund et al. 2008).

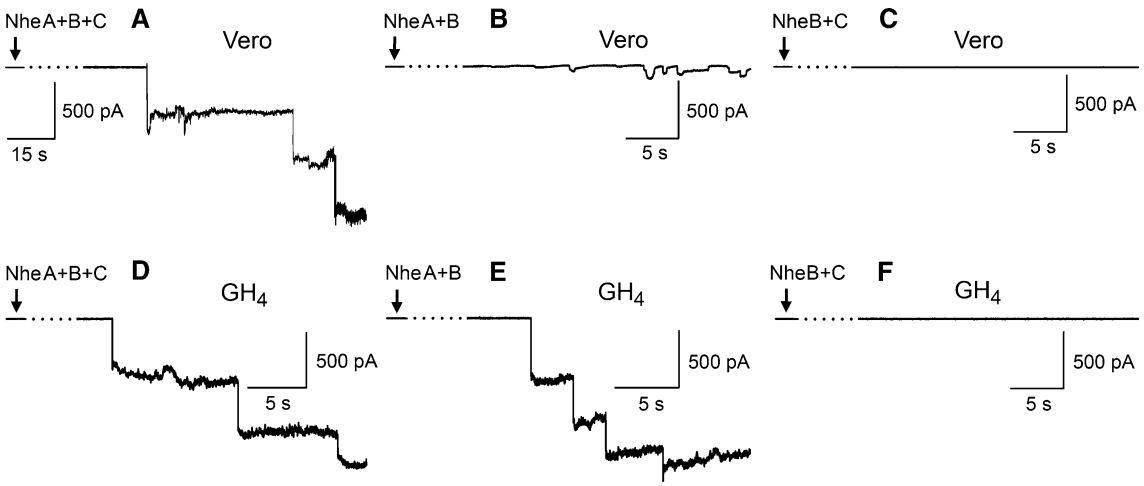

Fig. 6 Patch-clamp recordings from Vero and GH_4 cells exposed to NheA + B + C (NVH75/95), NheA + B (MHI1672) and NheB + C (MHI1761). Cells were voltage-clamped at a holding potential of −40 mV. Nhe was continuously pressure-ejected onto the cell from the time indicated by the *arrow*. After a delay of 1–3 min, exposure to NheA + B + C induced large current steps of approximately 400 pA in both Vero (**a**) and GH_4 (**d**) cells, indicating insertion of high-conductance channels in the membrane. NheA + B induced current steps of similar size in GH_4 cells (**e**) but much smaller steps in Vero cells (**b**). NheB + C had no effect on either of the tested cell types (**c**, **f**)

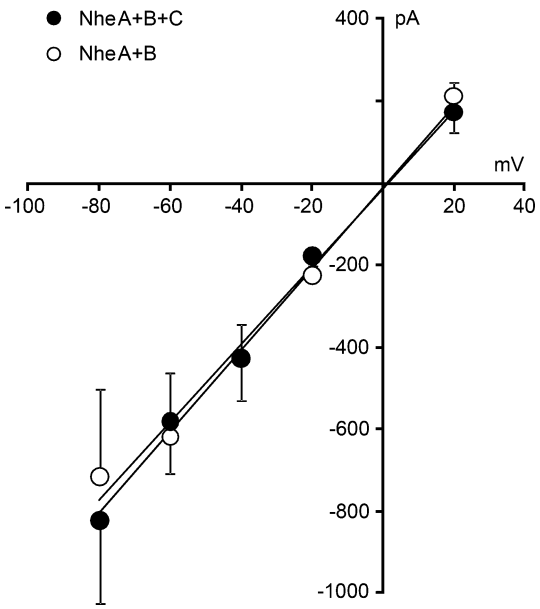

Fig. 7 *I–V* curves for the initial single-channel events in GH_4 cells after exposure to NheA + B + C (NVH75/95, *filled symbols*) and NheA + B (MHI1762, *open symbols*). Each point represents the average of the largest Nhe-induced current steps in five cells under voltage clamp. *Error bars* represent SD. The single-channel conductance estimated from the slope of the regression line is 10 nS for both toxin preparations

Discussion

By far the majority of the bacterial toxins that target the plasma membrane act as homo-oligomeric structures. While two-component PFTs have been described (the PV leukocidins of *S. aureus*), *B. cereus* has remained unusual in its use of at least two cytolysins that require three components, Nhe and Hbl. The data presented here show that this requirement for all three Nhe components in pore formation is dependent on cell type.

In this study, we used crude medium filtrate from different strains of *B. cereus*, producing only two of the three components, because purified Nhe components are not yet available. However, it appears likely that the reported effects are due to Nhe since these were abolished by a Mab against NheB which has been shown to lack cross-reactivity to other Nhe components (Dietrich et al. 2005). Similarly, this indicates that our results are not due to other PFTs, such as hemolysin II. Hemolysin II is a β-PFT resembling staphylococcal alpha toxin, and the channels formed by hemolysin II are weakly anion-selective, with a conductance of about 600 pS in 1 M KCl (Miles et al. 2002). Thus, these channels have a markedly smaller conductance than those formed by Nhe in either lipid bilayers or native cell membranes. For these reasons, we did not examine whether NVH 75/95 codes for hemolysin II and do not suspect any involvement of hemolysin II in the present study.

The results presented here exploit the recent identification and characterization of a set of distinct strains of *B. cereus* lacking expression of one of the three Nhe components (Lindback et al. 2010). The use of these naturally occurring strains was chosen as an alternative to generating isogenic mutants and assumes that the Nhe components are equally active. This assumption is supported by functional complementation of these strains; i.e., supplementing the culture supernatants with the missing Nhe component restores cytotoxicity (Lindback et al. 2010).

The aim of the present study was to explore the biophysical properties of Nhe in native cell membranes. In this context, the choice of kidney (Vero) and pituitary (GH_4) cell lines as preparations is reasonable, although the clinically relevant targets are human intestinal epithelia. GH_4 cells are very sensitive to Nhe and have the additional advantage of forming gigaseals easily with the patch electrodes. Vero cells are commonly used as a model system for testing bacterial toxins, and data from this cell line provide a reference to earlier studies on *B. cereus* toxins, including Nhe. Unexpectedly, our use of the two cell lines revealed that Nhe has cell type-specific effects.

The data showing that plasma membranes of Vero and GH_4 cells become permeable to both monovalent (K^+) and divalent (Ca^{2+}) cations when exposed to all three Nhe components are consistent with Nhe being able to establish channels in synthetic planar lipid bilayers (Fagerlund et al. 2008). However, the increased K^+ efflux detected in both Vero and GH_4 cells exposed to NheA + B alone (i.e., without NheC) suggests that a channel is formed by these two proteins alone, whereas in Vero cells NheC is still essential for permeabilizing the plasma membrane to Ca^{2+}. Due to its relatively high charge density and hydration energy, Ca^{2+} is generally a less permeant ion than K^+. Thus, our data indicate that the pore formed by Nhe is essentially a two-component structure, while NheC is required for maximum channel conductance in some cell types.

As NheB + C (MHI1761) was inert in all three assays (K^+ efflux, $[Ca^{2+}]_i$ and patch clamp), NheB appears unable to form a transmembrane pore by itself. Yet, there remains an absolute requirement for NheB in pore formation since activity of Nhe in Vero and GH_4 cells is abolished by Mab 1E11, raised against NheB. This finding excludes the possibility that NheA alone is able to form the large-conductance channel and agrees with our previous finding that deletion of NheB and NheC (i.e., a strain producing just NheA) abolished cytotoxic activity in Vero and Caco-2 cells (Fagerlund et al. 2008). The possibility that contaminating NheC is present in low amounts in the supernatant of *B. cereus* MHI1672 is also excluded since there is a stop codon mutation early in the gene for NheC and no trace of the protein can be detected in ELISA (Lindback et al. 2010).

The present report is the first to provide electrophysiological data on Nhe-induced channel formation in native cell membranes. The single-channel conductance of the largest Nhe channels was estimated to be 10 nS in normal physiological saline, which is more than ten times the 200–700 pS conductance of Nhe-inserted channels in planar lipid bilayers (Fagerlund et al. 2008). This difference in channel conductance in the two membrane environments is intriguing and leads to speculation that mammalian cell membranes contain proteins and/or lipids that function as receptors and/or alter the pore structure (perhaps through differing stoichiometry of the different components). In GH_4 cells, such inherent membrane components may act as a surrogate NheC since NheA + B alone inserted channels in GH_4 cells with identical conductance to that of the channels formed by NheA + B + C in Vero cells.

Endogenous plasma membrane ion channels yield single-channel conductances from <1 pS to around 250 pS in physiological saline. To our knowledge, the mammalian membrane channel with the largest conductance described to date is the mitochondrial apoptosis-induced channel (MAC), which has a peak conductance of 1.5–5 nS (Kinnally and Antonsson 2007). Bacterial PFTs insert channels that also vary in unitary conductance and in structure. The largest described to date are probably those formed by β-PFT cholesterol-dependent cytolysins, which are able to oligomerize as structures exceeding 35 monomers (Tweten 2005). Shepard et al. (2000) found that perfringolysin forms channels with 4–6 nS conductance in 0.2 M NaCl in planar lipid bilayers, approximately half that observed in the present study for Nhe channels in native cell membranes.

Of greater relevance are the electrophysiological findings for ClyA. Although no patch-clamp recordings of ClyA in epithelia have been reported, a conductance close to 10 nS in 1 M KCl for ClyA has been recorded in planar lipid bilayers. However, in 0.1 and 0.3 M KCl bathing solutions, the conductance is 1 and 3 nS, respectively (Ludwig et al. 1999). Thus, assuming a relatively nonspecific channel, ClyA is expected to have a conductance of around 1 nS in the quasi-physiological solutions used in the present study.

The relationship between the single-channel conductance (G), radius (r) and length (L) of a wide, unspecific channel in solution of conductivity σ (15.7 mS cm^{-1} for our experimental solutions) may be estimated using the formula

$$G = \sigma \pi r^2 / L$$

Assuming the length of the transmembrane-spanning region of membrane-inserted Nhe to be similar to that of ClyA, i.e., approximately 3 nm (Mueller et al. 2009), the diameter for the Nhe pore is estimated to be 5 nm ($r = 2.46$ nm). This size falls within the range 4–10 nm obtained for various ClyA pore structures in cryo EM reconstructions (Tzokov et al. 2006). The pore diameter of the membrane-bound crystal structure of ClyA is 4 nm (Mueller et al. 2009), matching that of a subset of cryo EM images (Tzokov et al. 2006). The fact that cryo EM of ClyA revealed pore structures of different size (suggested to represent oligomers of varying numbers [Tzokov et al. 2006]) may be of relevance to our finding of decreasing Nhe-induced current steps in patch-clamp recordings, indicating that the channel is not fixed in size. The reduction in current amplitude is unlikely to reflect

different oligomeric structures since the amplitudes of the initial single-channel events are similar for NheA + B + C (NVH75/95) and NheA + B (MHI1672).

In addition to functional similarities between Nhe and ClyA, notably both being able to form weakly cation-selective membrane channels (Fagerlund et al. 2008; Ludwig et al. 1999), structural homology of NheB and NheC to the related three-component hemolysin of *B. cereus*, Hbl, has identified significant structural features in common with ClyA (Fagerlund et al. 2008). The structure of ClyA as both aqueous and membrane-bound forms has been described and indicates a mechanism by which the dodecameric homo-oligomer rearranges to form a transmembrane pore (Mueller et al. 2009). However, while the ClyA channel consists of 12 identical subunits, the data given here indicate that the Nhe channel includes a minimum of two different proteins, NheA and NheB. How these subunits interact to form a channel is not known and restricts the extent to which one can extrapolate from the mechanism of ClyA to that of Nhe or Hbl.

Conclusion

We have shown that the Nhe toxin complex rapidly permeabilizes plasma membranes of mammalian cells by forming channels of about 10 nS conductance. To our knowledge, this is the largest channel conductance reported in native cell membranes under quasi-physiological conditions. In GH_4 cells, NheA + B are necessary and sufficient for insertion of large-conductance channels permeable to Ca^{2+}, whereas in Vero cells NheC is additionally required for insertion of such channels. In this cell type, NheA + B form K^+-permeant channels of lower conductance, indicating that Nhe is fundamentally a two-component toxin but that the third component (NheC) is necessary for full cytotoxicity in some cell types.

Acknowledgements We thank Richard Dietrich and Erwin Märtlbauer for supplying the Mab against NheB and the MHI1672 and MHI1761 strains of *B. cereus.*

References

Anderluh G, Lakey JH (2008) Disparate proteins use similar architectures to damage membranes. Trends Biochem Sci 33: 482–490

Arnesen LPS, Fagerlund A, Granum PE (2008) From soil to gut: *Bacillus cereus* and its food poisoning toxins. FEMS Microbiol Rev 32:579–606

Beecher DJ, Wong ACL (1994) Improved purification and characterization of hemolysin Bl, a hemolytic dermonecrotic vascular-permeability factor from *Bacillus cereus*. Infect Immun 62: 980–986

Dietrich R, Moravek M, Burk C, Granum PE, Martlbauer E (2005) Production and characterization of antibodies against each of the three subunits of the *Bacillus cereus* nonhemolytic enterotoxin complex. Appl Environ Microbiol 71:8214–8220

Fagerlund A, Lindback T, Storset AK, Granum PE, Hardy SP (2008) *Bacillus cereus* Nhe is a pore-forming toxin with structural and functional properties similar to the ClyA (HlyE, SheA) family of haemolysins, able to induce osmotic lysis in epithelia. Microbiology 154:693–704

Gonzalez MR, Bischofberger M, Pernot L, van der Goot FG, Freche B (2008) Bacterial pore-forming toxins: the (w)hole story? Cell Mol Life Sci 65:493–507

Hamill OP, Marty A, Neher E, Sakmann B, Sigworth FJ (1981) Improved patch-clamp techniques for high-resolution current recording from cells and cell-free membrane patches. Eur J Physiol 391:85–100

Kinnally KW, Antonsson B (2007) A tale of two mitochondrial channels, MAC and PTP, in apoptosis. Apoptosis 12:857–868

Lai XH, Arencibia I, Johansson A, Wai SN, Oscarsson J, Kalfas S, Sundqvist KG, Mizunoe Y, Sjostedt A, Uhlin BE (2000) Cytocidal and apoptotic effects of the ClyA protein from *Escherichia coli* on primary and cultured monocytes and macrophages. Infect Immun 68:4363–4367

Liebhaber H, Riordan JT, Horstmann DM (1967) Replication of rubella virus in a continuous line of African green monkey kidney cells (Vero). Proc Soc Exp Biol Med 125:636–643

Lindback T, Fagerlund A, Rodland MS, Granum PE (2004) Characterization of the *Bacillus cereus* Nhe enterotoxin. Microbiology 150:3959–3967

Lindback T, Hardy SP, Dietrich R, Sødring M, Didier A, Moravek M, Fagerlund A, Bock S, Nielsen C, Casteel M, Granum PE, Märtlbauer E (2010) Cytotoxicity of *Bacillus cereus* Nhe enterotoxin requires specific binding order of the three components. Infect Immun 78:3813–3821

Ludwig A, Tengel C, Bauer S, Bubert A, Benz R, Mollenkopf HJ, Goebel W (1995) SlyA, a regulatory protein from *Salmonella typhimurium*, induces a haemolytic and pore-forming protein in *Escherichia coli*. Mol Gen Genet 249:474–486

Ludwig A, Bauer S, Benz R, Bergmann B, Goebel W (1999) Analysis of the SlyA-controlled expression, subcellular localization and pore-forming activity of a 34 kDa haemolysin (ClyA) from *Escherichia coli* K-12. Mol Microbiol 31:557–567

Lund T, Granum PE (1996) Characterisation of a non-haemolytic enterotoxin complex from *Bacillus cereus* isolated after a foodborne outbreak. FEMS Microbiol Lett 141:151–156

Madegowda M, Eswaramoorthy S, Burley SK, Swaminathan S (2008) X-ray crystal structure of the B component of hemolysin BL from *Bacillus cereus*. Protein Struct Funct Bioinform 71: 534–554

Miles G, Bayley H, Cheley S (2002) Properties of *Bacillus cereus* hemolysin II: a heptameric transmembrane pore. Prot Sci 11:1813–1824

Montoya M, Gouaux E (2003) Beta-barrel membrane protein folding and structure viewed through the lens of alpha-hemolysin. Biochim Biophys Acta Biomembr 1609:19–27

Mueller M, Grauschopf U, Maier T, Glockshuber R, Ban N (2009) The structure of a cytolytic alpha-helical toxin pore reveals its assembly mechanism. Nature 459:726–730

Oscarsson J, Westermark M, Lofdahl S, Olsen B, Palmgren H, Mizunoe Y, Wai SN, Uhlin BE (2002) Characterization of a pore-forming cytotoxin expressed by *Salmonella enterica* serovars Typhi and Paratyphi A. Infect Immun 70:5759–5769

Parker MW, Feil SC (2005) Pore-forming protein toxins: from structure to function. Prog Biophys Mol Biol 88:91–142

Shepard LA, Shatursky O, Johnson AE, Tweten RK (2000) The mechanism of pore assembly for a cholesterol-dependent cytolysin: formation of a large prepore complex precedes the insertion of the transmembrane beta-hairpins. Biochemistry 39:10284–10293

Tashjian AH Jr, Yasumura Y, Levine L, Sato GH, Parker ML (1968) Establishment of clonal strains of rat pituitary tumor cells that secrete growth hormone. Endocrinology 82:342–352

Tweten RK (2005) Cholesterol-dependent cytolysins, a family of versatile pore-forming toxins. Infect Immun 73:6199–6209

Tzokov SB, Wyborn NR, Stillman TJ, Jamieson S, Czudnochowski N, Artymiuk PJ, Green J, Bullough PA (2006) Structure of the hemolysin E (HlyE, ClyA, and SheA) channel in its membrane-bound form. J Biol Chem 281:23042–23049

Usmani SM, Dietel P, Wittekindt OH (2010) Ca^{2+} signaling in alveolar epithelial cells by the pore forming cytolysin, streptolysin-O. Acta Physiol 198 (suppl 677): P-MON-72